Catalysis Science & Technology

PAPER

View Article Online
View Journal | View Issue

Cite this: *Catal. Sci. Technol.*, 2019, 9, 1289

Hierarchically constructed NiO with improved performance for catalytic transfer hydrogenation of biomass-derived aldehydes†

Jian He,[ab] Monia Runge Nielsen,[c] Thomas Willum Hansen,[c] Song Yang *[b] and Anders Riisager *[a]

Received 17th December 2018,
Accepted 11th February 2019

DOI: 10.1039/c8cy02536c

rsc.li/catalysis

A 3D nano-/micrometer-scaled NiO material with urchin-like structure was prepared *via* a facile, green synthesis route, and served as a highly efficient and durable catalyst for catalytic transfer hydrogenation (CTH) of bio-based furfural (FF) to furfuryl alcohol (FAOL) using 2-propanol as H-donor and solvent. The as-prepared NiO possessed a good active-site accessibility owing to a high surface area and large amount of acid–base sites, resulting in high FF conversion of 97.3% with 94.2% FAOL yield at 120 °C and 3 h of reaction, which was a superior catalytic performance compared to commercial NiO nanoparticles. Besides, the excellent catalytic performance of the sea urchin-like NiO was validated for gram-scale FAOL synthesis, and recyclability test confirmed the catalyst to be reusable for multiple reaction runs without significant activity loss after intermediary calcination in air. Notably, the introduced catalytic system was also applicable to CTH of alternative bio-derived aldehydes.

1 Introduction

Considerable attention is nowadays directed towards the development of renewable feedstock from biomass resources that can serve as substitutes for limited fossil-based resources for the production of bio-fuels and fine chemicals.[1–3] Furfural (FF), the acid-hydrolysis product of biomass-derived C5-based carbohydrates, is recognized as one of the most promising feedstock in the manufacture of a broad spectrum of fuels and valuable chemicals *via* upgrading strategies such as, *e.g.*, hydrogenation, hydrogenolysis and aldolization.[4–6] Furfuryl alcohol (FAOL), as a typical representative reduction derivative of FF, can serve as a versatile precursor in the synthesis of synthetic fibers, resins, adhesives and vitamin C,[7–10] and act as an intermediate linking C5-carbohydrates to the downstream products of bio-based furan derivatives (*e.g.*, levulinic acid and γ-valerolactone) (Scheme 1).[11,12] In this regard, hydrogenation of FF into FAOL has received widespread attention.

The multi-functionality of the FF molecule (*i.e.*, C=C, C=O and C–O) can result in several hydrogenation products such as FAOL, tetrahydrofurfuryl alcohol (TFAOL), 2-methylfuran (2-MF) and 2-methyltetrahydrofuran (2-MTHF).[13–15] This renders the selectivity formation of FAOL from FF a remaining challenging as low product yield is often obtained.[16,17] So far, many heterogeneous catalysts have been developed for the transformation of FF into FAOL using gaseous hydrogen as H-donor.[18–21] However, low reaction selectivity towards the target product and the potential danger of handling pressurized, external H_2 gas owing to its flammable and explosive properties coupled with the high cost of transportation and storage, encourage exploitation of alternative strategies for the production of FAOL from FF.[22] Recently, catalytic transfer hydrogenation (CTH) has emerged as a very interesting alternative approach using abundant, renewable and low-cost alcohol as combined H-donor and solvent during the process. This results in more safe and convenient operation in comparison with the direct use of gaseous H_2 as H-donor in terms of cost and handling.[23–26] Moreover, it is proven that carbonyl groups can be highly selectivity reduced to hydroxyl groups during the CTH process, which is strongly associated to the Meerwein–Ponndorf–Verley (MPV) reaction in organic chemistry.[27] Many heterogeneous catalysts have already been exploited for CTH of FF to FAOL with alcohol (Table S1†), but although substantial progression have been made most catalytic systems are generally subjected to

[a] *Centre for Catalysis and Sustainable Chemistry, Department of Chemistry, Technical University of Denmark, DK-2800 Kgs. Lyngby, Denmark. E-mail: ar@kemi.dtu.dk*
[b] *State Key Laboratory Breeding Base of Green Pesticide & Agricultural Bioengineering, Key Laboratory of Green Pesticide & Agricultural Bioengineering, Ministry of Education, State-Local Joint Laboratory for Comprehensive Utilization of Biomass, Center for Research & Development of Fine Chemicals, Guizhou University, Guiyang 550025, PR China. E-mail: jhzx.msm@gmail.com*
[c] *National Centre for Nano Fabrication and Characterization, Technical University of Denmark, DK-2800 Kgs. Lyngby, Denmark*

† Electronic supplementary information (ESI) available. See DOI: 10.1039/c8cy02536c

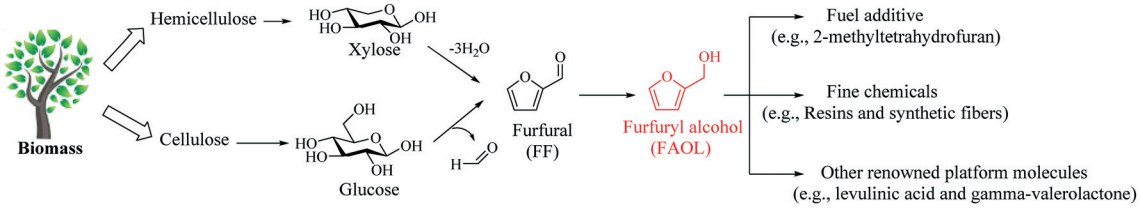

Scheme 1 Cascade synthesis of FAOL from bio-based carbohydrates and application of FAOL.

undesired harsh reaction conditions (*i.e.*, $T \geq 140$ °C and/or $t \geq 6$ h) and require large catalyst dosage to work efficiently. In addition, most of the reported catalysts involve tedious preparation procedures limiting their practical application. Thus, there is still great potential to improve the synthesis of FAOL from FF by CTH.

The structural features of solids, including morphology, surface area and component dispersion, have a significant influence on their catalytic performance.[28,29] In this perspective, 3D micro or nano-materials with hierarchical construction have shown outstanding activity in catalysis thanks to their large surface area, highly available active sites and improved mass transportation.[30] For instance, has flower-like Co_3O_4–CeO_2 composite demonstrated to be an efficient catalyst for the degradation of 1,2,4-trichlorobenzene,[31] flower-like MgO catalyst was efficient for dimethyl carbonate synthesis,[32] and 3D flower-like micro/nano Ce–Mo composite oxide has been developed as an efficient catalyst for one-pot transformation of fructose to 2,5-diformylfuran.[33]

In previous work,[34] we reported that commercially available $NiFe_2O_4$ nanoparticles could efficiently catalyze the CTH of FF to FAOL with 2-propanol. Following our continuous interesting in the development of highly efficient and low cost catalysts for the CTH of FF, we prepared in this study 3D sea urchin-like and flower-like NiO catalysts by facile and environmental-friendly methods without the use of strong base or pungent ammonia hydroxide. The 3D sea urchin-like NiO was thoroughly characterized by various techniques and demonstrated to be highly catalytically active for CTH of FF to FAOL with 2-propanol as H-donor, yielding 94.2% FAOL under mild reaction conditions (120 °C, 3 h).

2 Experimental

2.1 Materials

Nickel(II) chloride (98%), PEG–PPG–PEG pluronic P-123 ($M_{average}$ = 5800 g mol^{-1}), NiO (99.8%, <50 nm particle size), furfuryl alcohol (FAOL, 98%), 5-methylfurfural (5-MFF, 99%), naphthalene (>99%, internal standard), benzaldehyde (>99%), benzyl alcohol (≥99%), 4-methoxybenzaldehyde (98%), 4-methoxybenzyl alcohol (98%), 3,4-dimethoxybenzaldehyde (99%), 3,4-dimethoxybenzyl alcohol (96%), 2,4,6-trimethylbenzaldehyde (98%), 2,4,6,-trimethylbenzyl alcohol (99%), cinnamic alcohol (98%), heptanal (≥95%), 2-propanol (99.5%), methanol (≥99.8%), ethanol (99.5%) and acetone (≥99%) were purchased from Sigma-Aldrich. Cinnamaldehyde (>98%) was received from Merck. 5-Hydroxymethylfurfural (HMF, ≥95%), 2,5-furandicarboxaldehyde (DFF, ≥95%), 5-methylfuran-2-methanol (≥95%) and 2,5-furandimethanol (≥95%) were obtained from Bepharm Ltd. Urea (≥99%), furfural (FF, ≥99%), 2-butanol (≥99.5%), *tert*-butyl alcohol (≥99.7%) and *n*-heptanol (>99%) were procured from Fluka.

2.2 Catalyst preparation

In a typical synthesis, 1.296 g (10 mmol) $NiCl_2$, 1.80 g (30 mmol) urea and 2.5 g pluronic P-123 were dissolved in deionized water (80 mL) with magnetic stirring (500 rpm) at room temperature for 2 h. The resulting green transparent solution was then transferred into a 200 mL Teflon lined stainless steel autoclave and heated at 90 °C for 12 h. Subsequently, the autoclave was quickly cooled to room temperature in a water bath, the green product collected by filtration followed by washing with deionized water until the pH of the filtrate was neutral following by drying at 80 °C in air for 5 h (86% yield of solid). Finally, the as-prepared sample was calcined at 300 or 400 °C in air for 4 h and the obtained catalyst were denoted as NiO(P)-300 or NiO(P)-400, respectively. For comparison, NiO-300 was prepared according to the above described procedure but in the absence of pluronic P-123.

2.3 Catalyst characterization

Powder X-ray diffraction (XRD) patterns of samples were acquired on a Huber G670 diffractometer with Cu Kα radiation (λ = 0.154184 nm) and recorded in the 2θ range from 5 to 80°. N_2 adsorption–desorption measurements were completed on a Micromeritics ASAP 2020 instrument, wherein the samples were firstly degassed at 200 °C in vacuum for 4 h and adsorption–desorption isotherms subsequently acquired at −196 °C. The Brunauer–Emmett–Teller (BET) method was applied to evaluate the specific surface area of the samples. Thermal gravimetric (TG) analysis of samples were performed on a METTLER TOLEDO thermal analyzer in dynamic air atmosphere (30 mL min^{-1}) in the temperature range 25–600 °C with a heating rate of 10 °C min^{-1}. NH_3/CO_2-Temperature programmed desorption (TPD) measurements of samples were conducted on a Micromeritics AutoChem II 2920 apparatus equipped with a thermal conductivity detector (TCD). Prior to TPD analysis, the samples were heated at 300 °C under a He flow (25 mL min^{-1}) for 1 h, subjected to a mixture of NH_3/CO_2–He gas flow (15 mL min^{-1}) for 1 h at 50

°C followed by flushing with pure He gas (25 mL min^{-1}) to remove physically adsorbed NH_3/CO_2. Finally, the desorption of NH_3/CO_2 were performed by heating the samples to 300 °C at a rate of 10 °C min^{-1} and maintaining it here for 1 h. SEM (scanning electron microscopy) images of samples were recorded on a FEI Nova NANO SEM 600 with the thru-the-lens camera with an accelerating voltage at 5 kV. TEM (transmission electron microscopy) images were recorded on a FEI Tecnai T20 G2 microscope at 200 kV with a LaB6/CeB6 Thermionic filament. X-ray photoelectron spectroscopy (XPS) spectra of samples were recorded on a ThermoScientific K-Alpha spectrometer with Al Kα radiation (1484.6 eV), in which C 1s at 284.8 eV was applied as calibration peak. Metal leaching from the NiO(P)-300 catalyst in the filtrate after reaction was determined by inductively coupled plasma optical emission mass spectrometry (ICP-MS) on a Thermo Scientific iCAP Q ICP-MS with the aid of acid digests.

2.4 Catalytic activity test and product analysis

The CTH of FF was performed in 15 mL ACE pressure tube equipped with magnetically driven stirrer and oil-bath. In brief, 0.096 g (1 mmol) FF, specified amount of catalyst (0.005–0.03 g), 5 mL 2-propanol (as H-donor and solvent), and 0.02 g naphthalene (as internal standard) were mixed in the reactor. After sealing, the reactor was placed in a preheated oil bath (100–140 °C) for a specific reaction time at a stirring rate of 500 rpm (time zero when the reactor was immersed in the oil bath). After the desired time of reaction, the reactor was quickly cooled to room temperature in a water bath. Aliquot of the reaction mixtures was quantitatively analyzed by GC (Agilent 6890N) fitted with FID detector, wherein the FF conversion and FAOL yield were calculated on basis of standard curves of commercially pure compounds. Furthermore, the liquid products in the reaction mixture were identified by GC-MS (Agilent 6850-5975C). Both the GC and the GC-MS was equipped with a HP-5MS capillary column (30.0 m × 250 μm × 0.25 μm).

The recyclability of the NiO(P)-300 catalyst was tested over six consecutive reaction runs at 120 °C with a reaction time of 3 h. For the first four runs, the used catalyst was after each run separated by centrifugation, washed with ethanol and acetone (5 mL) in sequence, subsequently dried at 80 °C for 2 h and then used for the next run. For the fifth and sixth recycle runs, catalyst regeneration were achieved by calcination in air at 300 °C for 4 h. Product analysis was performed as described above.

The CTH of other aldehydes was performed in a similar way as described above, but with a 50 mL stainless steel autoclave with mechanical stirring (500 rpm) using 2 mmol substrate, 0.06 g catalyst, 10 mL 2-propanol and reaction temperature of 140 or 150 °C.

3 Results and discussion

3.1 Catalyst characterization

XRD patterns obtained of the as-prepared catalysts and commercial NiO nanoparticles are shown in Fig. 1a. NiO(P)-400 and commercial NiO had five characteristic peaks at 2θ = 37.3, 43.2, 62.7, 75.4 and 79.4°, which are indexed as (111), (200), (220), (311) and (222) planes of the crystalline rhombohedral phase of NiO,[35,36] respectively, consistent with JCPDS card 44-1159. In contrast, only three of the characteristic peaks were clearly observed for the samples of NiO(P)-300 and NiO-300, indicating less crystallinity of NiO when calcined at lower temperature.

Nitrogen physisorption isotherms of the catalyst samples measured by the BET method (Fig. 1b) showed type IV isotherms with H3-type hysteresis loop, implying that irregular mesoporous structures formed between the particles. The obtained BET surface areas of the samples are compiled in Table 1. As expected, higher calcination temperature greatly diminished the surface area of the as-prepared NiO (entries 2 and 3, Table 1). Besides, the surface area of NiO(P)-300 was larger than that of NiO-300 (entries 2 and 4, Table 1), revealing that the addition of pluronic P-123 during the course of preparation increased the surface area of the formed material.

The morphologies of the as-prepared catalysts were visualized by SEM and TEM analysis (Fig. 2). The SEM image of

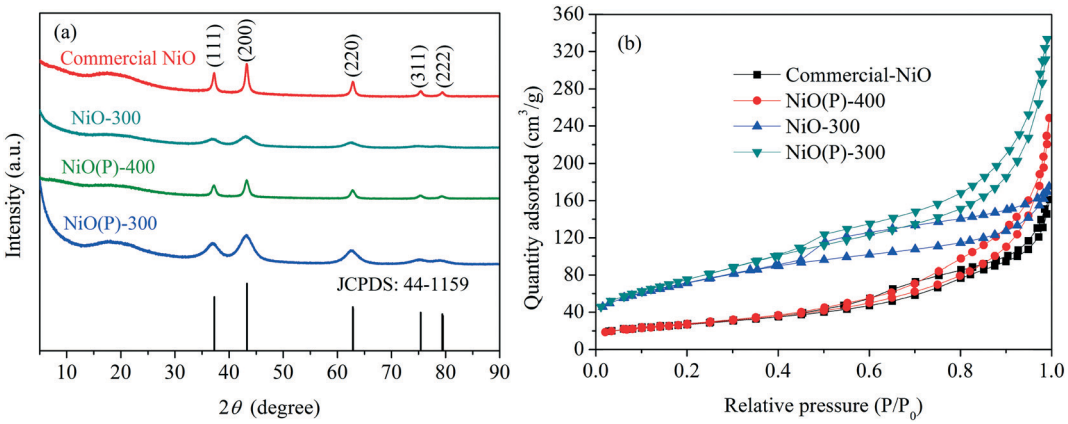

Fig. 1 (a) XRD patterns and (b) N_2 adsorption–desorption isotherms of the as-prepared catalysts and NiO nanoparticles.

Table 1 BET surface areas and acidity/basicity of the different catalysts

Entry	Catalyst	BET surface area[a] (m^2 g^{-1})	Acid amount[b] (mmol g^{-1})	Base amount[b] (mmol g^{-1})
1	Commercial NiO	94.8	0.192	0.059
2	NiO(P)-300	273.8	0.918	0.072
3	NiO(P)-400	95.5	0.303	0.065
4	NiO-300	257.8	0.923	0.080

[a] BET surface areas were determined by N_2 physisorption. [b] Acidity and basicity were evaluated by NH_3- and CO_2-TPD, respectively.

NiO(P)-300 (Fig. 2a) revealed a well-defined 3D nanometer-scale structure, which was assembled from a core with many densely arranged nano-needles as "spikes". The 3D nanometer-scale structure of NiO(P)-300 was clearly confirmed by its TEM image (Fig. 2b) consisting of a core of about 120 nm in diameter with "spikes" having diameters of about 50 nm. Thus, the construction of the NiO(P)-300 catalyst looked like "sea urchin". NiO(P)-400 possessed less pronounced sea urchin appearance, which seemed to be destroyed at increased calcination temperature. Instead it presented an agglomerated shape (Fig. 2c and d), which could account for the lower surface area of NiO(P)-400 (entry 3, Table 1) compared to NiO(P)-300. Fig. 2e and f showed that the construction units of NiO-300 were 3D hierarchical flower-like structures with diameters in the range of 1.2–1.4 μm, which were composed of many densely packed nanosheets like "petals". The distinct differences in catalyst construction between NiO(P)-300 and NiO-300 reflected that pluronic P-123 significantly influenced the catalyst structure during the course of preparation by decreasing the size of particles as well as enlarging the surface area.

The acid and base properties of the catalysts were further measured using NH_3- and CO_2-TPD (Fig. S1 and S2†). As shown in Table 1, the acidity and basicity of the NiO catalysts were strongly associated to the calcination temperature as evident from the NiO(P)-300 and NiO-300 samples, which possessed almost the same amount of acid and base sites (entries 2 and 4, Table 1), while NiO(P)-400 in comparison had less acid and base sites (entry 3, Table 1).

Furthermore, the Ni species in NiO(P-300) and commercial NiO nanoparticles were examined by XPS analysis. The XPS spectra of the Ni $2p_{3/2}$ region (Fig. 3) exhibited a main peak at about 854 eV and an associated satellite peak at about 861 eV for both NiO(P-300) and commercial NiO nanoparticles.[35,37] Overall, four deconvoluted peaks were needed to reproduce the shape of the Ni $2p_{3/2}$ signal, where the peaks at about 854.0 and 855.5 eV in the main peak region were characteristic of Ni^{2+} species and the other two deconvoluted peaks located at six to eight eV higher binding energy relative to the main peaks (*i.e.*, 854.0 and 855.5 eV) are generally assigned to satellite peaks.[37,38] No peak at 852.6 eV assignable to metallic Ni[38] was observed in either of the samples.

3.2 Catalyst evaluation for CTH of FF

Initial investigations were commenced by using the as-prepared NiO catalysts for CTH of FF to FAOL in 2-propanol at 120 °C (Table 2). A reference experiment confirmed that the formation of FAOL did not take place without catalyst present (entry 1, Table 2). In contrast, considerable amount of FAOL formed using the different NiO catalysts (entries 2–5, Table 2), confirming that the acid–base properties of the metal oxides were capable of facilitating the CTH reaction relying on MPV reduction.[39–41] Especially, 72.6% FF conversion with 70.2% FAOL yield (96.7% selectivity) was obtained in the presence of NiO(P)-300 under mild reaction conditions (120 °C, 1 h) resulting in a high FAOL formation rate of 585 $\mu molg^{-1}$ min^{-1} and a relatively high TOF value of 2.6 h^{-1} (entry 2, Table 2). The excellent catalytic performance of NiO(P)-300 was attributed to a combination of high surface area (273.8 m^2 g^{-1}) and high concentration of acid (0.918 mmol g^{-1}) and base sites (0.072 mmol g^{-1}) (entry 2, Table 1). Notably, the catalytic behavior of NiO(P)-300 far outperformed commercial NiO nanoparticles (FAOL formation rate of 142 $\mu molg^{-1}$ min^{-1} and TOF of 0.6 h^{-1}) (entry 5, Table 2). Similarly, good results were also obtained with NiO-300 which possessed a relative high surface area and equally many acid and base sites as NiO(P)-300, affording 56.9% yield of FAOL (90.7% selectivity) along with a FAOL formation rate of 474 $\mu molg^{-1}$ min^{-1} and a TOF value of 2.1 h^{-1} (entry 4, Table 2). Hence, both as-prepared NiO with sea urchin (*i.e.*, NiO(P)-300) or flower (*i.e.*, NiO-300) construction exhibited superior performance to commercial NiO nanoparticles with a mean particle size of about 15 nm (Fig. S3†) in the CTH of FF to FAOL, possibly as a consequence of their special constructions in combination with large density of acid–base sites. Noteworthy, as-prepared NiO with flower construction (*i.e.*, NiO-300) afforded a slightly lower selectivity toward FAOL compared to the other tested NiO catalysts (entries 2–5, Table 2). This was likely associated to the large particle size of NiO-300 as evidenced from Fig. S4,† in well agreement with nano-catalysis offering excellent selectivity.[22,42] As the as-prepared nanometer-scaled NiO with sea urchin construction (*i.e.*, NiO(P)-300) showed the best catalytic performance, this catalyst was selected for further study.

3.3 CTH of FF with NiO(P)-300

Effect of temperature, time, H-donor alcohol and catalyst dosage. The catalytic results obtained from CTH of FF with NiO(P)-300 by variation of reaction temperature and reaction time are presented in Fig. 4a. Increased reaction temperature or prolonged reaction time led to an increase in FF conversion and FAOL yield, while the FAOL selectivity remained

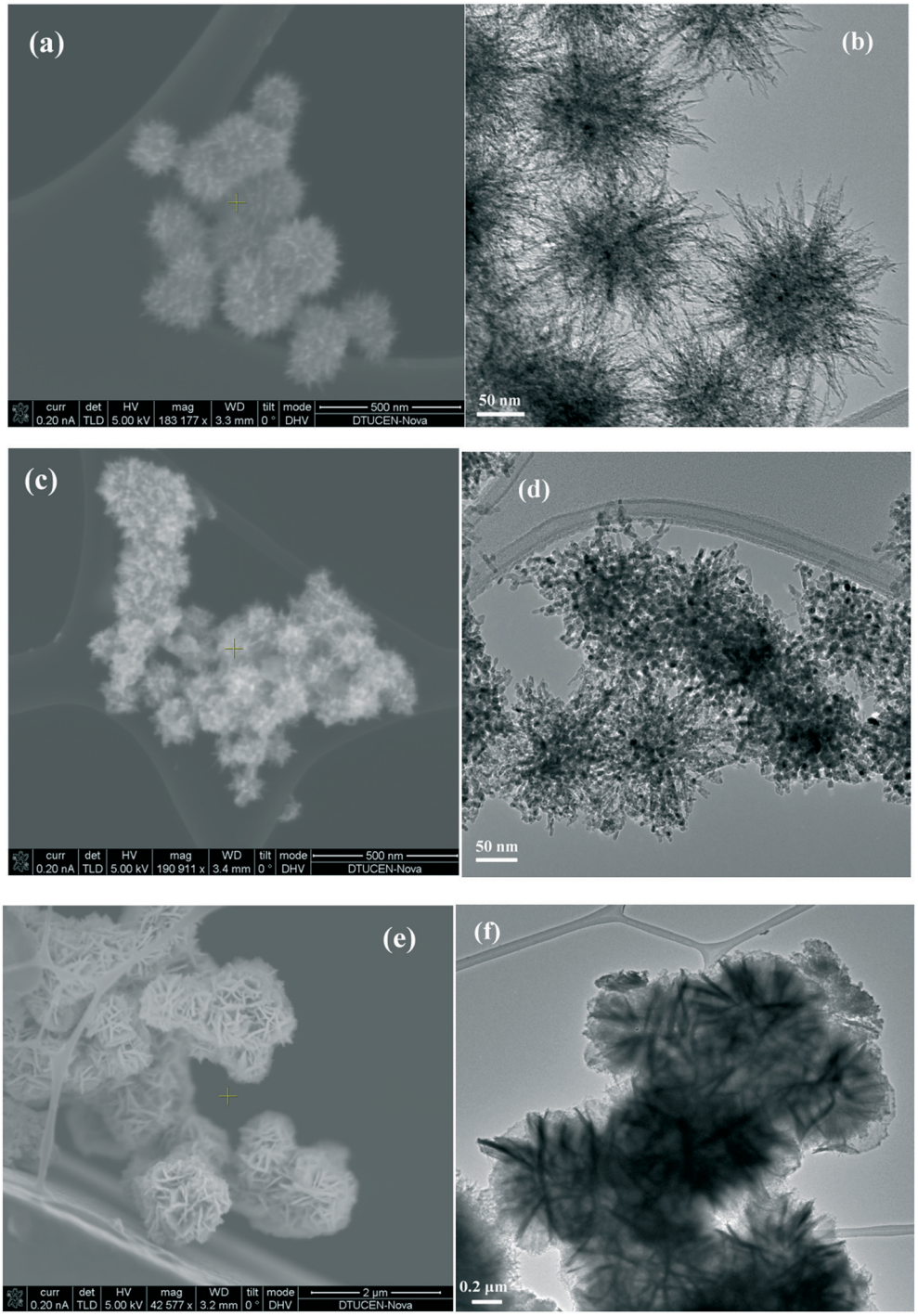

Fig. 2 (a) SEM image of NiO(P)-300; (b) TEM image of NiO(P)-300; (c) SEM image of NiO(P)-400; (d) TEM image of NiO(P)-400; (e) SEM image of NiO-300; (f) TEM image of NiO-300.

over 95% as clearly verified by the GC chromatograms of the reaction mixture (Fig. S5a†). Also, trace amount of 2-(diisopropoxymethyl)furan formed from acetalization of FF with 2-propanol was detected at the different reaction temperatures (Fig. S5b†). As high as 88.9% yield of FAOL along with 91.8% FF conversion was attained even at 100 °C with a reaction time of 5 h, signifying the excellent catalytic performance of NiO(P)-300. The great performance of the catalyst system was associated to a relative low activation energy (41.8 kJ mol^{-1}) (Fig. S6 and Table S2†), which was slightly lower than previously reported catalyst systems for CTH of FF to FAOL (Table S1†). Almost complete FF conversion was achieved at 120 °C after 4 h of reaction or at 140 °C after 2 h of reaction (Fig. 4a), clearly demonstrating that increased reaction temperature shortened the required reaction time to afford full FF conversion. Noteworthy, the reaction carried

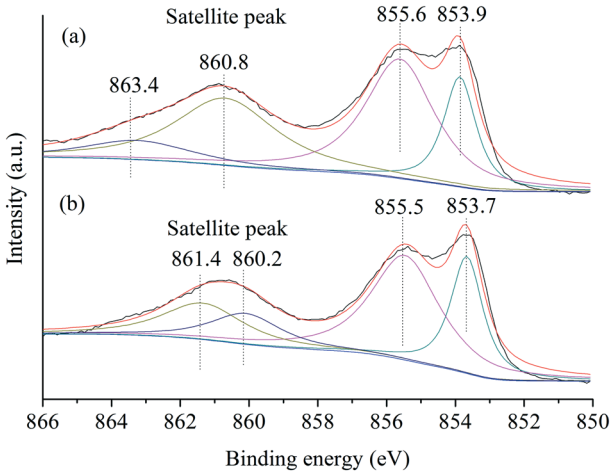

Fig. 3 XPS spectra of Ni $2p_{3/2}$ of (a) NiO(P)-300 and (b) commercial NiO samples.

out at 120 °C for 3 h offered 97.3% FF conversion and 94.2% FAOL yield, which were chosen as preferred conditions for further optimization.

Variation of the alcohol acting as solvent and H-donor in the tested system had a significant effect on the catalytic behavior (Fig. 4b). No FAOL was formed using *tert*-butanol as the reaction media, confirming that it could not facilitate CTH. On the other hand, excellent FAOL selectivities were achieved with 2-propanol and 2-butanol, confirming the good H-donating capability of secondary alcohols. Notably, a moderate FF conversion was observed at 120 °C in 2-butanol while ~90% FF conversion was achieved at 160 °C (Table S3†). This difference was probably a consequence of the relatively high viscosity and/or steric hindrance effect of 2-butanol compared to the other alcohols (*e.g.*, 2-propanol), resulting in relatively large mass dispersion limitation at low reaction temperature (120 °C). At higher reaction temperature (*e.g.*, 160 °C) where the viscosity of 2-butanol is significantly lower[43,44] the effect was less important. Ethanol performed also good as solvent/H-donor (75.4% yield of FAOL, 209 $\mu molg^{-1}\ min^{-1}$ of FAOL formation rate), however superior result (94.2% yield of FAOL, 262 $\mu molg^{-1}\ min^{-1}$) was observed with 2-propanol as preferred H-donor solvent.

The effect of NiO(P)-300 dosage on the CTH of FF at 120 °C was subsequently studied and the results are shown in Fig. 4c. No FAOL product was formed without added catalyst into the reaction system, as expected. In contrast, FF conversion and FAOL yield increased with increasing catalyst dosage and reached 97.3 and 94.2%, respectively, when the mass ratio of FF to catalyst was 4.8 : 1 (*i.e.*, use of 0.02 g catalyst). Further increase in catalyst dosage to 0.03 g (*i.e.*, mass ratio of FF to catalyst of 3.2 : 1) only marginally increased the yield to 95.5% after 3 h, but resulted in high FAOL yield (*e.g.*, 85.7%) within a shorter time (*e.g.*, 1 h). Also, the FAOL selectivity increased with increasing catalyst dosage, and the relative low FAOL selectivity at lower catalyst dosage was attributed to competing acetalization of FF with 2-propanol as revealed from GC-MS analysis.

Catalyst recycling. Prior to recycling experiments, the heterogeneous nature of the NiO(P)-300 catalyst was evaluated for the CTH reaction by a filtration experiment, where the catalyst was removed after 1 h reaction and the filtrate allowed to continue reaction under identical reaction conditions (120 °C) for an additional hour (Fig. S7†). The FAOL yield was periodically monitored and the FAOL yield remained around 70% with time with no nickel detected in the filtrate by ICP-MS analysis, which clearly indicated that the NiO(P)-300 catalyst was heterogeneous in nature and therefore likely prone to recycling.

Upon recycling, a gradual decline in FF conversion and FAOL yield was, however, observed for the first four reaction runs (Fig. 5a) resulting in moderate FF conversion and FAOL yield of 41.5 and 36.9%, respectively, while the FAOL selectivity maintained around 95%. Notably, the catalyst activity could be recovered almost completely after regeneration by calcination at 300 °C in air, which resulted in FAOL yield of 88.3 and 86.8% after the fifth and sixth reaction run, respectively, when applying intermediate calcination. Thus in-depth characterization of used and generated catalysts were conducted with an attempt to shed light on the reason of activity variation during the recycling experiments.

XRD (Fig. 5b) and XPS analysis (Fig. S8†) of the spent and regenerated catalysts revealed no crystallographic changes compared to the fresh catalyst and no reduced Ni species (no characteristic metallic Ni peak at 852.6 eV), respectively, strongly confirming that reduction of Ni^{2+} did not take place during the reaction. Besides, SEM and TEM analysis (Fig. 5c and d) confirmed preservation of the sea urchin-like constructions in the used samples, while ICP-MS analysis confirmed negligible nickel leaching (<0.5 ppm) into the filtrate after 3 h at 120 °C. Combined, this firmly demonstrated

Table 2 Catalytic performance of NiO catalysts for CTH of FF[a]

Entry	Catalyst	Conv. (%)	Yield (%)	Select. (%)	FAOL formation rate[b] ($\mu molg^{-1}\ min^{-1}$)	TOF[c] (h^{-1})
1	None	4.5	0.0	0.0	—	—
2	NiO(P)-300	72.6	70.2	96.7	585	2.6
3	NiO(P)-400	11.2	10.4	92.9	87	0.4
4	NiO-300	62.7	56.9	90.7	474	2.1
5	Commercial NiO	17.7	17.0	96.0	142	0.6

[a] Reaction conditions: 1 mmol FF, 0.02 g catalyst, 5 mL 2-propanol, 120 °C, 1 h. [b] Calculated from the FAOL yield obtained after 1 h. [c] Turnover frequency (TOF) as (mole of FAOL)/(mole of catalyst × reaction time).

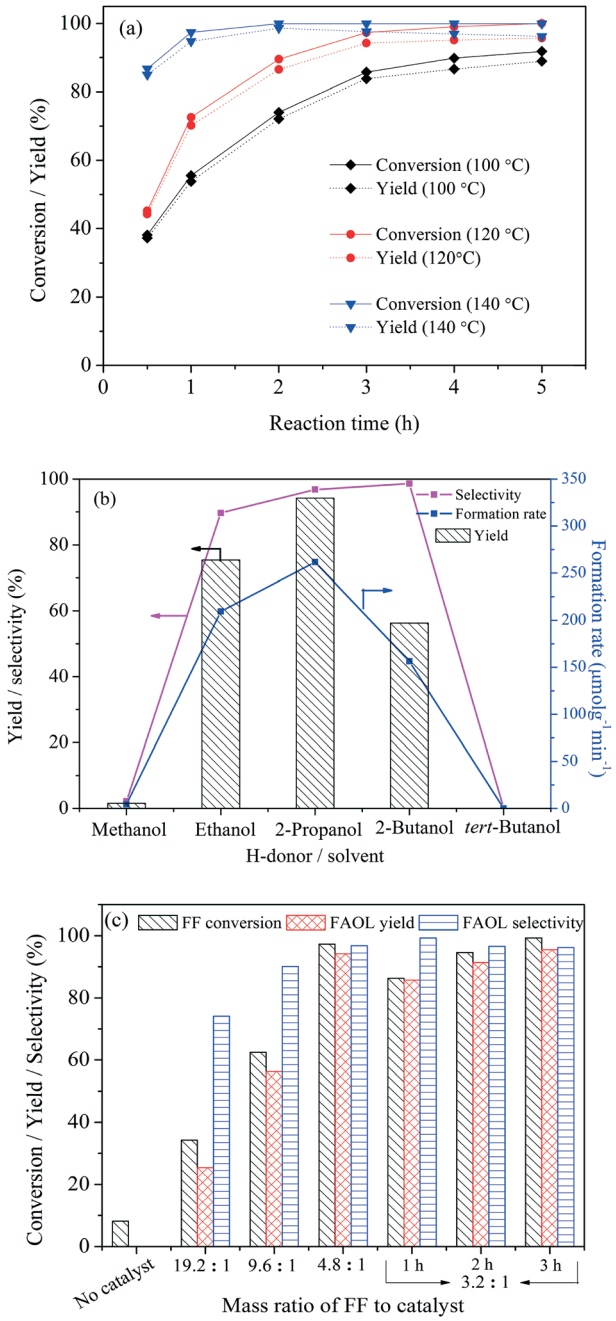

Fig. 4 (a) Effect of reaction temperature and reaction time on CTH of FF to FAOL (1 mmol FF, 0.02 g NiO(P)-300, 5 mL 2-propanol); (b) effect of alcohol as H-donor on CTH of FF to FAOL (1 mmol FF, 0.02 g NiO(P)-300, 5 mL alcohol, 120 °C, 3 h, formation rate calculated from the FAOL yield obtained after 3 h); (c) effect of catalyst dosage on the CTH of FF to FAOL (1 mmol FF, 5 mL 2-propanol, 120 °C, 3 h, mass ratio of FF to catalyst ranging from 19.2 to 3.2).

that the NiO(P)-300 catalyst was stable during the reaction. However, a significant weight loss was indeed found by TG analysis for the used catalyst in comparison to the fresh and regenerated catalysts (Fig. 5e), and an apparent color change was also observed (Fig. S9†). Retrospectively, it is speculated that organic residues adsorbed on the surface of the NiO(P)-300 catalyst resulted in the loss of activity and calcination at 300 °C restored the catalyst activity. This deduction was validated by the variation in the surface areas of the fresh (273.8 $m^2\ g^{-1}$), used (228.5 $m^2\ g^{-1}$) and regenerated catalyst (246.4 $m^2\ g^{-1}$) (Fig. 5f).

Scale-up and substrate scope. To evaluate the effectiveness of the NiO(P)-300 catalyst, a gram-scale CTH reaction was performed employing 20 mmol (1.92 g) FF at 140 °C as illustrated in Scheme S1.† The FF conversion was monitored by GC to be near quantitative after 5 h, where after 1.68 g (85.7% yield) of analytically pure (verified by NMR analysis in Fig. S10†) FAOL was obtained after filtration and rotary evaporation, implying that NiO(P)-300 possessed a promising potential for large-scale production of FAOL from FF *via* the CTH process.

In addition to FF, NiO(P)-300 was successfully employed for CTH of various other aldehydes, including α,β-unsaturated carbonyls, as shown from the results listed in Table 3. For instance, were excellent yields (92.8–97.4%) of the corresponding reduction products obtained in CTH of 2,5-furandicarboxaldehyde (entry 3), benzaldehyde (entry 4), 4-methoxybenzaldehyde (entry 5), 3,4-dimethoxybenzaldehyde (entry 6) and heptanal (entry 9) under relative mild reaction conditions (≤150 °C). Although lower conversions were observed for other aldehydes (entries 1, 2, 7 and 8), excellent selectivities of the corresponding reduction products were attained confirming that the NiO(P)-300 catalyst had good versatility in the CTH of aldehydes.

Inspired by the general excellent catalytic performance of NiO(P)-300 in CTH, we further attempted to use NiO(P)-300 combined with other acid catalysts for one-pot transformation of FF to alkyl levulinate, which is hailed as another versatile feedstock for the manufacture of bio-fuels and chemicals.[11] Since isopropyl levulinate (IPL) was not commercially available, pure IPL was prepared according to the method reported by Geboers *et al.*[45] and the purity confirmed by NMR analysis (Fig. S11†). As shown in Table S4,† nearly full FF conversion was achieved over NiO(P)-300 at 140 °C after 2 h of reaction, and the conversion of formed FAOL into IPL was subsequently catalyzed by common acid catalysts such as, *e.g.* Amberlyst 15, H-Beta, H-ZSM-5, H-MOR and H-Y. Eventually, a IPL yield of 61.5% was obtained from FF over NiO(P)-300 and Amberlyst 15 at 140 °C after 6 h in a two-step procedure, which is close to previously reported results.[46] The superior activity found for Amberlyst 15 compared to zeolites was mainly attributed to its larger amount of acidic sites and stronger acidity (Table S4†). In line with this, the dominant product from reaction with H-Beta (12.5) was the precursor of IPL, *i.e.* 2-(isopropoxymethyl)furan, derived from etherification of FAOL with 2-propanol. In contrast, IPL was the main product in the presence of Amberlyst 15 as its large amount of acidic sites and strong acidity further facilitated the transformation into IPL (Fig. S12†). In addition to the acid amount and acid strength, the narrow channels of zeolites constituting relatively large diffusion limitation probably also contributed to their low catalytic performance.[46] Anyway, the results clearly demonstrated the

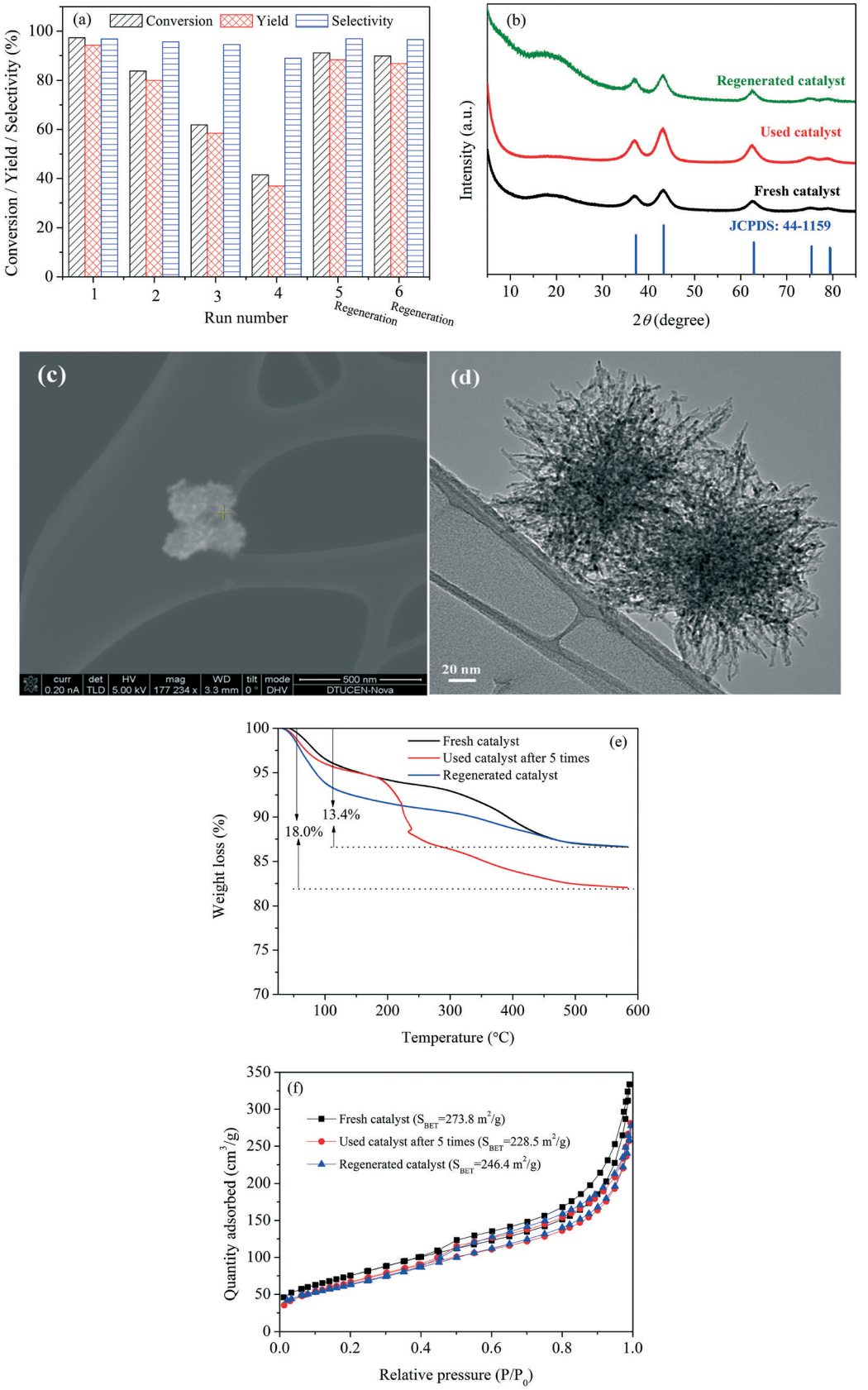

Fig. 5 (a) Catalytic performance of NiO(P)-300 in the CTH of FF to FAOL during recycling. (b) XRD patterns of fresh, used and regenerated NiO(P)-300 catalysts. (c) SEM image of used NiO(P)-300 catalyst. (d) TEM image of used NiO(P)-300 catalyst. (e) TG curves of fresh, used and regenerated NiO(P)-300 catalysts. (f) N_2 adsorption–desorption isotherms of fresh, used and regenerated NiO(P)-300 catalysts. Reaction conditions: 1 mmol FF, 0.02 g NiO(P)-300, 5 mL 2-propanol, 120 °C, 3 h.

Table 3 CTH of alternative aldehydes with NiO(P)-300[a]

Entry	Substrate	Product	Temp. (°C)	Time (h)	Conv. (%)	Yield (%)	Sel. (%)
1[b]		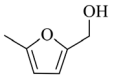	150	5	60.5	58.1	96.0
2[b]	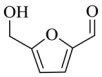	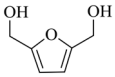	150	4	77.9	73.5	94.4
3[b]	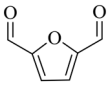	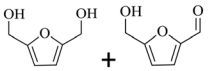	150	4	>99	79.6 (16.7)[c]	96.3
4		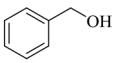	140	3	96.5	95.7	99.2
5	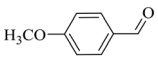	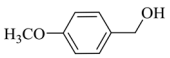	150	2	>99	97.1	98.1
6	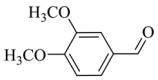	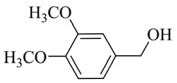	150	2	>99	97.4	98.4
7	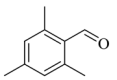	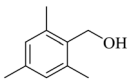	150	8	46.1	45.2	98.0
8	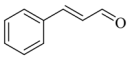	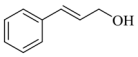	140	8	71.6	70.5	98.5
9	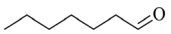	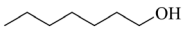	150	3	96.2	92.8	96.5

[a] Reaction conditions: 2 mmol substrate, 0.06 g NiO(P)-300, 10 mL 2-propanol. [b] 1 mmol substrate. [c] HMF yield.

potential of NiO(P)-300 to be employed in further upgrading of biomass-derived compounds with the combination of other type of catalysts, further supporting the versatility of NiO(P)-300.

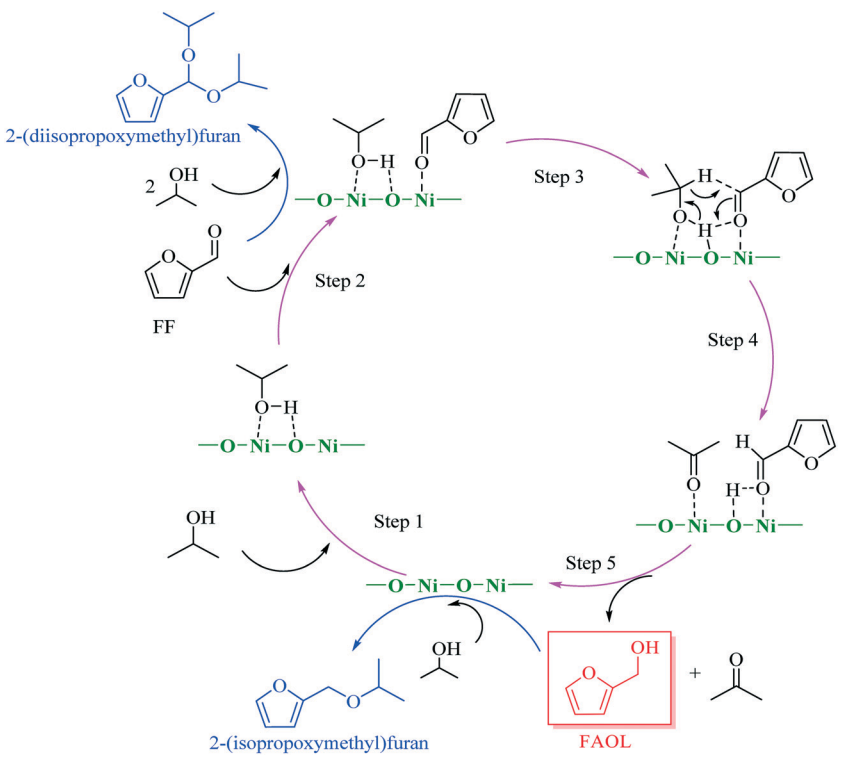

Scheme 2 Plausible reaction mechanism for the CTH of FF to FAOL with NiO(P)-300 in 2-propanol.

Table 4 Comparison of the catalytic performance of NiO(P)-300 with other Ni-based catalysts in the production of FAOL from FF with alcohols as H-donor

Entry	Catalyst	Cat. reduction	Cat. amount[a] (wt%)	$C_{initial}$ FF[b] (mol L^{-1})	H-Donor	Temp. (°C)	Time (h)	Conv. (%)	Yield (%)	Select. (%)	Ref.
1	Ni–Ru/C	600 °C/N_2/3 h	28.9	0.36	Benzyl alcohol	150	12	—	81.1	—	51
2	Ni–Cu/Al_2O_3	320 °C/15 bar H_2/3 h	22.3	1.17	2-Propanol	200	4	95.4	95.4	100	52
3	Ni/Fe_2O_3	No reduction	33.3	0.40	2-Propanol	180	7.5	46	33	71.7	53
4	Ni–Cu	250 °C/1 bar H_2/1 h	40.0	0.43	2-Propanol	110	2.3	50	50	100	54
5	5% Ni/AC	450 °C/1 bar H_2/1 h	12.5	0.42	2-Propanol	260	5	95	20	21.1	55
6	10% Ni–15% W/AC	450 °C/1 bar H_2/3 h	12.5	0.42	2-Propanol	260	5	83	25	30.1	55
7	$NiFe_2O_4$	No reduction	31.2	0.2	2-Propanol	180	6	99	94	94.9	34
8	NiO(P)-300	No reduction	20.8	0.2	2-Propanol	120	3	97.3	94.2	96.8	[c]

[a] Relative to initial mass of FF. [b] Initial molar concentration of FF. [c] This work.

CTH reaction mechanism. To get more insight into the mechanism of CTH of FF over NiO(P)-300, poisoning experiments were conducted by adding benzoic acid[47] or piperidine[48] into the reaction system with the aim of poisoning base or acid sites of the NiO(P)-300 catalyst, respectively (Table S5†). The results clearly showed that addition of either benzoic acid or piperidine led to significant reductions in FAOL yield, initial FAOL formation rate as well as TOF value, implying the remarkable catalytic performance of NiO(P)-300 was strongly associated with the synergic role of acidic–basic sites within the catalyst.

The results obtained from the above characterization and catalytic testing in combination with knowledge from literature[22,23,26,27] allowed us to propose a plausible reaction mechanism for the CTH process with NiO(P)-300, assuming that the mechanism was associated to MPV reduction facilitated by acidic (Ni^{2+}) and basic sites (O^{2-}). As delineated in Scheme 2, 2-propanol was adsorbed to the surface of NiO(P)-300 catalyst and then activated by acidic–basic sites (Ni^{2+}–O^{2-}) within the catalyst to give 2-propoxide, while the carbonyl group in FF was concomitantly activated by acidic sites (Ni^{2+}). Next, H-transfer between activated FF and generated 2-propoxide occurred involving a six-member intermediate on the surface of the catalyst forming FAOL and acetone. Normally, minor amount of 2-(diisopropoxymethyl)furan was observed throughout the studies as a by-product (Fig. S5†), generated by acetalization of FF with 2-propanol over acidic sites of the catalyst. Additionally, trace amount of 2-(isopropoxymethyl)furan, originated from etherification of FAOL with 2-propanol over acidic sites of the catalyst, was detected when the reaction took place in presence of a large amount of NiO(P)-300 catalyst (*i.e.*, 0.03 g) with long reaction time (*i.e.*, ≥3 h).

It is well-known that Ni-based catalysts, preferable RANEY® Ni,[49,50] are efficient catalysts for transfer hydrogenation/hydrogenolysis using alcohols as H-donor, and several Ni-based catalysts have already been reported for CTH of FF to FAOL as compiled in Table 4.[51–55] Notably, the NiO(P)-300 catalyst developed in this work exhibited however superior catalytic performance in CTH of FF to FAOL compared to previously reported Ni-based catalysts. Specifically, the NiO(P)-300 catalyst did not require pre-reduction and H_2 gas (or high temperature carbon reduction under inert gas) could therefore be omitted during catalyst preparation making the process cost-effective. Therefore, the facile, low-cost and green preparation method together with high catalytic performance render the developed NiO(P)-300 catalyst a promising substitute of Ni(0)-based catalysts for CTH.

4 Conclusions

In this work, 3D hierarchical structures of NiO catalysts (sea urchin- and flower-like) have successfully been prepared *via* a facile yet environmental-friendly hydrothermal method in the absence of strong or stimulating alkali supply, and demonstrated to be highly active for CTH of FF to FAOL using 2-propanol as both H-donor and solvent. The 3D hierarchical construction and low calcination temperature (300 °C) contributed to high surface area and large amount of acid–base sites as well as facile active-site accessibility in the catalysts, which were found to play critical roles in the efficient production of FAOL from CTH of FF. A high FF conversion of 91.8% along with 88.9% FAOL yield was achieved under very mild reaction conditions (100 °C, 5 h) using the sea urchin-like NiO(P)-300 catalyst, and FF conversion and FAOL yield were increased to 97.3 and 94.2%, respectively, at 120 °C after only 3 h. Moreover, the effectiveness and heterogeneous nature of the catalyst were confirmed by a low value of activation energy (41.8 kJ mol^{-1}), successful gram-scale testing, one-pot conversion of FF into IPL in combination with Amberlyst 15 and filtration experiment, respectively. In addition, the catalyst proved reusable several times without significant activity loss after facile regeneration by calcination (300 °C, in air). Importantly, the catalytic system proved also applicable to CTH of various other aldehydes. In perspective, we envisage the low-cost and efficient catalyst prepared by a green strategy in this work to be a potentially attractive catalyst for industrial CTH of FF as well as other aldehydes.

Conflicts of interest

There are no conflicts to declare.

Acknowledgements

JH gratefully acknowledges financial support from The Chinese State Scholarship (No. 201606670008), SY acknowledges the

National Natural Science Foundation of China (No. 21576059 and 21666008), and AR acknowledges the Department of Chemistry, Technical University of Denmark for support.

References

1 T. Renders, S. V. den Bosch, S. Koelewijn, W. Schutyser and B. F. Sels, *Energy Environ. Sci.*, 2017, **10**, 1551–1557.
2 H. Li, S. Yang, S. Saravanamurugan and A. Riisager, *ACS Catal.*, 2017, **7**, 3010–3029.
3 H. Li, A. Riisager, S. Saravanamurugan, A. Pandey, R. S. Sangwan, S. Yang and R. Luque, *ACS Catal.*, 2018, **8**, 148–187.
4 L. Zhang, G. Xi, Z. Chen, D. Jiang, H. Yu and X. Wang, *Chem. Eng. J.*, 2017, **307**, 868–876.
5 S. S. Chen, T. Maneerung, D. C. W. Tsang, Y. S. Ok and C. Wang, *Chem. Eng. J.*, 2017, **328**, 246–273.
6 K. Tomishige, Y. Nakagawa and M. Tamura, *Green Chem.*, 2017, **19**, 2876–2924.
7 S. T. Thompson and H. H. Lamb, *J. Catal.*, 2017, **350**, 111–121.
8 W. Gong, C. Chen, Y. Zhang, H. Zhou, H. Wang, H. Zhang, Y. Zhang, G. Wang and H. Zhao, *ACS Sustainable Chem. Eng.*, 2017, 2172–2180.
9 P. N. Romano, J. M. A. R. de Almeida, Y. Carvalho, P. Priecel, E. F. Sousa-Aguiar and J. A. Lopez-Sanchez, *ChemSusChem*, 2016, **9**, 3387–3392.
10 Z. Zhang, J. Song, Z. Jiang, Q. Meng, P. Zhang and B. Han, *ChemCatChem*, 2017, **9**, 2448–2452.
11 E. Jorge, T. D. M. Lima, C. Lima, L. Marchini, W. N. Castelblanco, D. G. Rivera, E. A. Urquieta-González, R. S. Varma and M. W. Paixao, *Green Chem.*, 2017, **19**, 3856–3868.
12 S. Song, L. Di, G. Wu, W. Dai, N. Guan and L. Li, *Appl. Catal., B*, 2017, **205**, 393–403.
13 Z. Jiang, W. Wan, Z. Lin, J. Xie and J. G. Chen, *ACS Catal.*, 2017, **7**, 5758–5765.
14 N. Pino, S. Sitthisa, Q. Tan, T. Souza, D. López and D. E. Resasco, *J. Catal.*, 2017, **350**, 30–40.
15 X. Chang, A. Liu, B. Cai, J. Luo, H. Pan and Y. Huang, *ChemSusChem*, 2016, **9**, 3330–3337.
16 P. T. Sulmonetti, S. H. Pang, M. T. Claure, S. Lee, D. A. Cullen, P. K. Agrawal and C. W. Jones, *Appl. Catal., A*, 2016, **517**, 187–195.
17 L. Grazia, D. Bonincontro, A. Lolli, T. Tabanelli, C. Lucarelli, S. Albonetti and F. Cavani, *Green Chem.*, 2017, **19**, 4412–4422.
18 J. Wu, G. Gao, J. Li, P. Sun, X. Long and F. Li, *Appl. Catal., B*, 2017, **203**, 227–236.
19 J. J. Musci, A. B. Merlo and M. L. Casella, *Catal. Today*, 2017, **296**, 43–50.
20 S. M. Rogers, C. R. A. Catlow, C. E. Chan-Thaw, A. Chutia, N. Jian, R. E. Palmer, M. Perdjon, A. Thetford, N. Dimitratos, A. Villa and P. P. Wells, *ACS Catal.*, 2017, **7**, 2266–2274.
21 C. P. Jiménez-Gómez, J. A. Cecilia, D. Durán-Martín, R. Moreno-Tost, J. Santamaría-González, J. Mérida-Robles, R. Mariscal and P. Maireles-Torres, *J. Catal.*, 2016, **336**, 107–115.
22 G. Wang, X. Deng, D. Gu, K. Chen, H. Tüysüz, B. Spliethoff, H. Bongard, C. Weidenthaler, W. Schmidt and F. Schüth, *Angew. Chem., Int. Ed.*, 2016, **55**, 11101–11105.
23 H. Li, J. He, A. Riisager, S. Saravanamurugan, B. Song and S. Yang, *ACS Catal.*, 2016, **6**, 7722–7727.
24 M. J. Gilkey and B. Xu, *ACS Catal.*, 2016, **6**, 1420–1436.
25 J. He, H. Li, A. Riisager and S. Yang, *ChemCatChem*, 2018, **10**, 430–438.
26 L. Hu, T. Li, J. Xu, A. He, X. Tang, X. Chu and J. Xu, *Chem. Eng. J.*, 2018, **352**, 110–119.
27 M. Koehle and R. F. Lobo, *Catal. Sci. Technol.*, 2016, **6**, 3018–3026.
28 B. P. Bastakoti, H. Huang, L. Chen, K. C. Wu and Y. Yamauchi, *Chem. Commun.*, 2012, **48**, 9150–9152.
29 M. Ko, L. Mendecki and K. A. Mirica, *Chem. Commun.*, 2018, **54**, 7873–7891.
30 S. Zhang, H. Gao, J. Li, Y. Huang, A. Alsaedi, T. Hayat, X. Xu and X. Wang, *J. Hazard. Mater.*, 2017, **321**, 92–102.
31 S. Lin, G. Su, M. Zheng, D. Ji, M. Jia and Y. Liu, *Appl. Catal., B*, 2012, **123–124**, 440–447.
32 Z. Cui, Z. Chen, C. Cao, W. Song and L. Jiang, *Chem. Commun.*, 2013, **49**, 6093–6095.
33 Z. Yang, W. Qi, R. Su and Z. He, *ACS Sustainable Chem. Eng.*, 2017, **5**, 4179–4187.
34 J. He, S. Yang and A. Riisager, *Catal. Sci. Technol.*, 2018, **8**, 790–797.
35 M. A. Peck and M. A. Langell, *Chem. Mater.*, 2012, **24**, 4483–4490.
36 C. Yuan, X. Zhang, Q. Wu and B. Gao, *Solid State Ionics*, 2006, **177**, 1237–1242.
37 S. Song, S. Yao, J. Cao, L. Di, G. Wu, N. Guan and L. Li, *Appl. Catal., B*, 2017, **217**, 115–124.
38 H. W. Nesbitt, D. Legrand and G. M. Bancroft, *Phys. Chem. Miner.*, 2000, **27**, 357–366.
39 M. J. Gilkey, P. Panagiotopoulou, A. V. Mironenko, G. R. Jenness, D. G. Vlachos and B. Xu, *ACS Catal.*, 2015, **5**, 3988–3994.
40 A. Prasertsab, J. A. Cecilia, C. P. Jiménez-Gómez, C. García-Sancho, R. Moreno-Tost and P. Maireles-Torres, *Appl. Catal., A*, 2018, **556**, 1–9.
41 N. S. Biradar, A. M. Hengne, S. S. Sakate, R. K. Swami and C. V. Rode, *Catal. Lett.*, 2016, **146**, 1611–1619.
42 V. Polshettiwar and R. S. Varma, *Green Chem.*, 2010, **12**, 743–754.
43 H. Habibi, A. Hekmat-Nazemi, A. Kamran-Pirzaman and A. H. Mohammadi, *J. Mol. Liq.*, 2016, **220**, 558–565.
44 C. K. Zéberg-Mikkelsen, S. E. Quiñones-Cisneros and E. H. Stenby, *Fluid Phase Equilib.*, 2002, **194–197**, 1191–1203.
45 J. Geboers, X. Wang, A. B. de Carvalho and R. Rinaldi, *J. Mol. Catal. A: Chem.*, 2014, **388–389**, 106–115.
46 M. Paniagua, J. A. Melero, J. Iglesias, G. Morales, B. Hernández and C. López-Aguado, *Appl. Catal., A*, 2017, **537**, 74–82.
47 X. Tang, H. Chen, L. Hu, W. Hao, Y. Sun, X. Sun, L. Lin and S. Liu, *Appl. Catal., B*, 2014, **147**, 827–834.
48 V. A. Ivanov, J. Bachelier, F. Audry and J. C. Lavalley, *J. Mol. Catal.*, 1994, **91**, 45–59.

49 Z. Yang, Y. Huang, Q. Guo and Y. Fu, *Chem. Commun.*, 2013, **49**, 5328–5330.
50 X. Wang and R. Rinaldi, *Energy Environ. Sci.*, 2012, **5**, 8244–8260.
51 Z. Gao, L. Yang, G. Fan and F. Li, *ChemCatChem*, 2016, **8**, 3769–3779.
52 H. P. R. Kannapu, C. A. Mullen, Y. Elkasabi and A. A. Boateng, *Fuel Process. Technol.*, 2015, **137**, 220–228.
53 D. Scholz, C. Aellig and I. Hermans, *ChemSusChem*, 2014, **7**, 268–275.
54 S. A. Khromova, M. V. Bykova, O. A. Bulavchenko, D. Y. Ermakov, A. A. Saraev, V. V. Kaichev, R. H. Venderbosch and V. A. Yakovlev, *Top. Catal.*, 2016, **59**, 1413–1423.
55 Y. Wang, P. Prinsen, K. S. Triantafyllidis, S. A. Karakoulia, A. Yepez, C. Len and R. Luque, *ChemCatChem*, 2018, **10**, 3459–3468.